Electronic Supplementary Information:

Suppressing the formation of NO_x and N_2O in a CO_2/N_2 dielectric barrier discharge plasma by adding CH_4: Scavenger chemistry at work

Ramses Snoeckx,[1,2] Karen Van Wesenbeeck,[3] Silvia Lenaerts,[3] Min Suk Cha[1] and Annemie Bogaerts[2]

[1]King Abdullah University of Science and Technology (KAUST), Clean Combustion Research Center (CCRC), Physical Science and Engineering Division (PSE), Thuwal 23955, Saudi Arabia

[2]Research group PLASMANT, Department of Chemistry, University of Antwerp, Universiteitsplein 1, BE-2610 Antwerp, Belgium

[3]Research group DuEL, Department of Bioscience Engineering, University of Antwerp, Antwerp, Belgium

E-mail: ramses.snoeckx@kaust.edu.sa

Table of Contents

List of Figures

List of Tables

1. Materials and methods

1.1. Plasma reactor

Experiments were carried out in a coaxial DBD reactor, consisting of a stainless steel mesh (high voltage electrode) wrapped over the outside of a quartz tube with an outer diameter of 22 mm and an inner diameter of 16.5 mm. A stainless steel rod with an outer diameter of 13 mm, placed at the center of the tube, was used as ground electrode. The length of the discharge region was 90 mm, with a discharge gap of 1.75 mm, resulting in a discharge volume of 7.4 cm^3. The DBD reactor was powered by an AC high-voltage power supply (AFS, custom made), providing a maximum peak-to-peak voltage of 40 kV and a variable frequency of 1–90 kHz. CO_2, N_2, and CH_4 (Air Liquide, Alphagaz 1, 99.999 %) were used as feed gases, with a total flow rate of 611 mL min^{-1}. The CO_2:N_2 ratio and the CH_4 content were controlled independently with mass flow controllers (Bronkhorst, EL-Flow select F-210CV). The reactor was operated at atmospheric temperature and pressure. The total current was recorded by a Rogowski-type current monitor (Pearson 4100), and a high voltage probe was used to measure the applied voltage. The voltage on the external capacitor (10 nF) was also recorded in order to obtain the charge generated in the discharge. Finally, all the electrical signals were sampled by a four-channel digital oscilloscope (Picotech PicoScope 64201), and the discharge power was obtained using a control system that calculates the area of the Q-U Lissajous figures. The specific energy input (SEI) was based on the plasma power divided by the total gas flow rate (120 W / 611 $mL \cdot min^{-1}$ = 12 kJ L^{-1}).

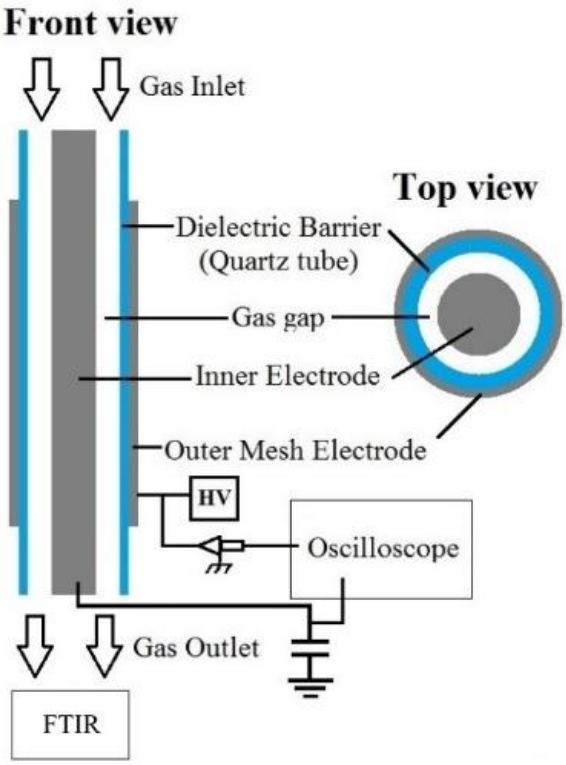

Figure S1. Schematic diagram of the experimental setup.

1.2. Product analysis

We applied Fourier transform infrared spectroscopy (FTIR; Thermo Fischer Scientific, Nicolet 380) to study the formation of NO_x compounds (i.e., NO, NO_2, N_2O_3 and N_2O_5) and N_2O. By inserting a 2-m IR gas cell in the FTIR spectrometer, we obtained an IR absorption spectrum showing all IR active vibrations. During the experiments, an FTIR resolution of 1 cm^{-1} was used, resulting in a spectrum being taken every 15 s. FTIR bands corresponding to an IR active functional group of the gases were monitored. Figure S4 shows the spectrum for a 1:1 mixture CO_2:N_2 without the addition of CH_4. For basic qualitative measurements, this technique provides close-to-real-time information on gas phase production of the N-containing compounds.

2. Detailed results

This section provides detailed information on the input conditions and results.

2.1. Experimental input conditions

Table S1. Overview of the compositions of the various gas mixtures used in the experiments.

	CO_2	N_2	CH_4	CO_2	N_2	CH_4	CO_2:N_2	Power
No.	*mL/min*	*mL/min*	*mL/min*	*%*	*%*	*%*	*Ratio*	*Watt*
E0	305	305	0	50	50	0	1:1	120
CH_4 addition				*CH_4 addition*				
E1	305	306	0.78	49.89	49.98	0.13	1:1	120
E2	305	304	1.59	49.86	49.89	0.25	1:1	120
E3	304	304	3.11	49.72	49.77	0.51	1:1	120
E4	303	303	4.60	49.59	49.65	0.75	1:1	120
E5	302	302	6.09	49.47	49.53	1.00	1:1	120
E6	302	302	7.00	49.43	49.43	1.15	1:1	120
E7	301	301	9.18	49.22	49.28	1.50	1:1	120
E8	300	299	12.36	49.04	48.93	2.02	1:1	120

2.2. Experimental results for CH_4 addition

Table S2. Overview of the different FTIR absorbance logging bands for experiments with addition of CH_4.

	NO	**NO_2**	**N_2O**	**CO**	**CH_3OH**	**HCN**	**NH_3**
FTIR band	1875.5	1598.8	2233.3	2144.1	1033.7	3334.0	996.7
No.	*a.u.*	*a.u.*	*a.u.*	*a.u.*	*a.u.*	*a.u.*	*a.u.*
E0	0.154	0.192	0.175	0.203	-0.001	-0.002	0.000
CH_4 addition							
E1	0.089	0.130	0.248	0.117	-0.003	0.001	-0.001
E2	0.089	0.111	0.252	0.109	-0.002	0.003	-0.006
E3	0.087	0.068	0.298	0.117	0.001	0.010	-0.002
E4	0.076	0.059	0.331	0.118	0.008	0.013	-0.002
E5	0.076	0.034	0.362	0.137	0.017	0.002	0.007
E6	0.076	0.025	0.359	0.136	0.018	0.023	0.004
E7	0.067	0.011	0.420	0.154	0.038	0.041	0.020
E8	0.057	0.008	0.465	0.166	0.088	0.063	0.098

Table S3. Overview of the CH_4 conversion, based on the FTIR absorbance at 3028 cm^{-1}, for experiments with added CH_4.

	Blank		**Measurement**		
	CH_4 conc.	**absorbance**	**absorbance**	**CH_4 conc.**	**CH_4 conv.**
No.	*%*	*a.u.*	*a.u.*	*%*	*%*
E0	0.00	0.000	-0.001	0.00	N.A.
CH_4 addition					
E1	0.128	0.072	-0.002	0.00	100.0
E2	0.254	0.106	-0.001	0.00	100.0
E3	0.509	0.175	0.024	0.014	97.2
E4	0.753	0.180	0.048	0.053	92.9
E5	0.998	0.219	0.070	0.110	89.0
E6	1.146	0.240	0.086	0.162	85.9
E7	1.502	0.279	0.142	0.423	71.8
E8	2.021	0.322	0.202	0.828	59.0

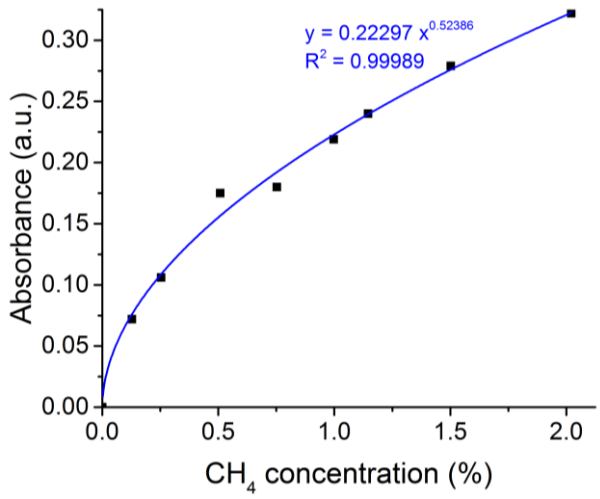

Figure S2. Correlation between the CH_4 concentration and the FTIR absorbance of CH_4 at 3028 cm^{-1}, for blank measurements with added CH_4.

The correlation between the known added CH_4 concentration and the FTIR absorbance of CH_4 at 3028 cm^{-1} for the blank measurements (see Figure S2) allowed us to estimate the conversion of CH_4 during our experiments, by correlating the absorbance measured at 3028 cm^{-1} for the plasma measurements with the CH_4 concentration, using the following function:

$$y = 0.22297 \cdot x^{0.52386} \Leftrightarrow x = \left(\frac{y}{0.22297}\right)^{\frac{1}{0.52386}} \quad \text{(eq.1)}$$

The obtained CH_4 concentration was then used, together with the original CH_4 concentration, to calculate the conversion of CH_4 (see Table S3). From Table S3 and Figure S3, it is clear that upon adding more CH_4 the CH_4 conversion starts to decrease and upon adding more than 0.75 to 1.00 % CH_4 (the stoichiometric amount) the conversion starts decreasing more rapidly. In Figure S3 this can be seen through the asymptotic fit through the effective CH_4 conversion.

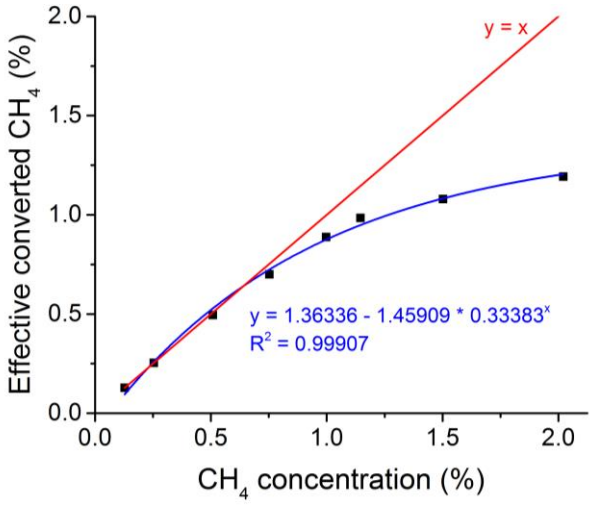

Figure S3. Correlation between CH_4 concentration and the effectiveness of the conversion of CH_4; the red line indicates the case in which all the added CH_4 is completely converted.

2.3. FTIR spectra

FTIR data were obtained by first subtracting the spectra from a blank measurement taken before the plasma was turned on, and then subtracting the spectrum taken for H_2O.

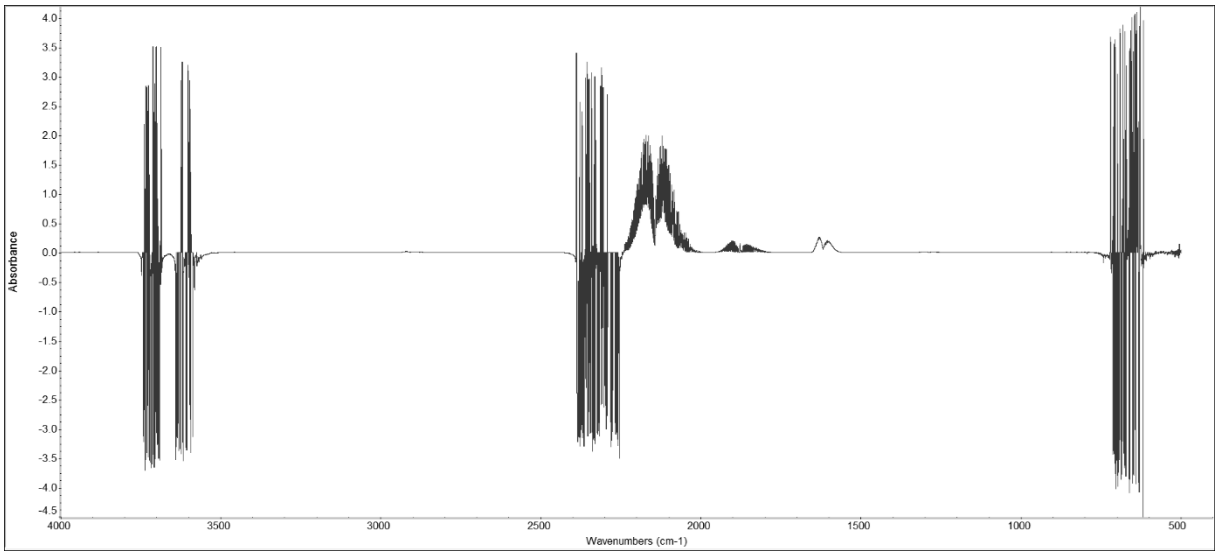

Figure S4. FTIR spectrum of E0, 1:1 mixture CO_2:N_2 without CH_4 added.

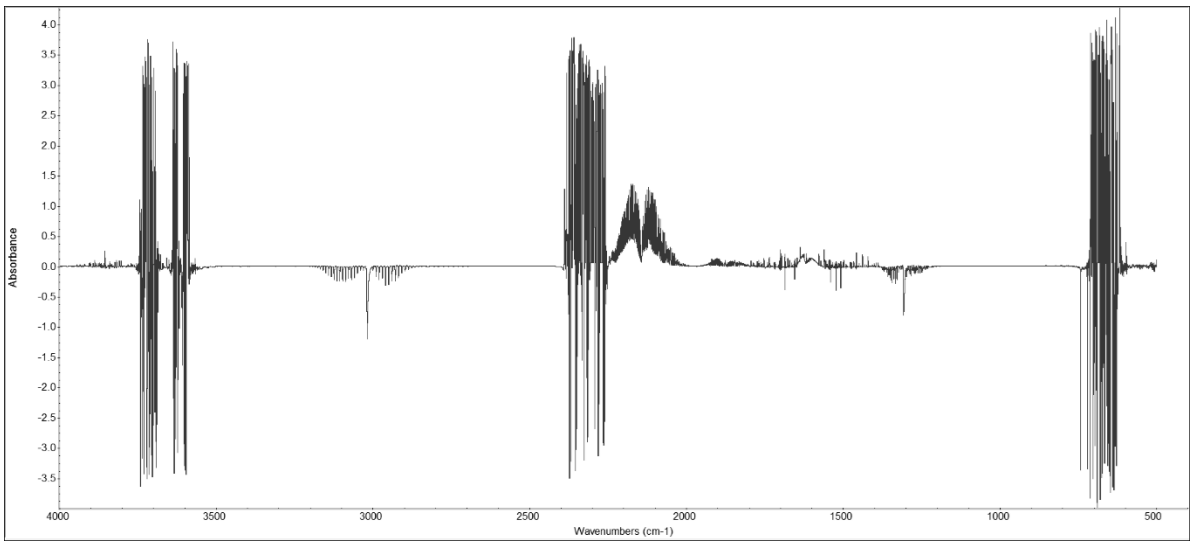

Figure S5. FTIR spectrum of E1, 1:1 mixture CO_2:N_2 with 0.13 % CH_4 added.

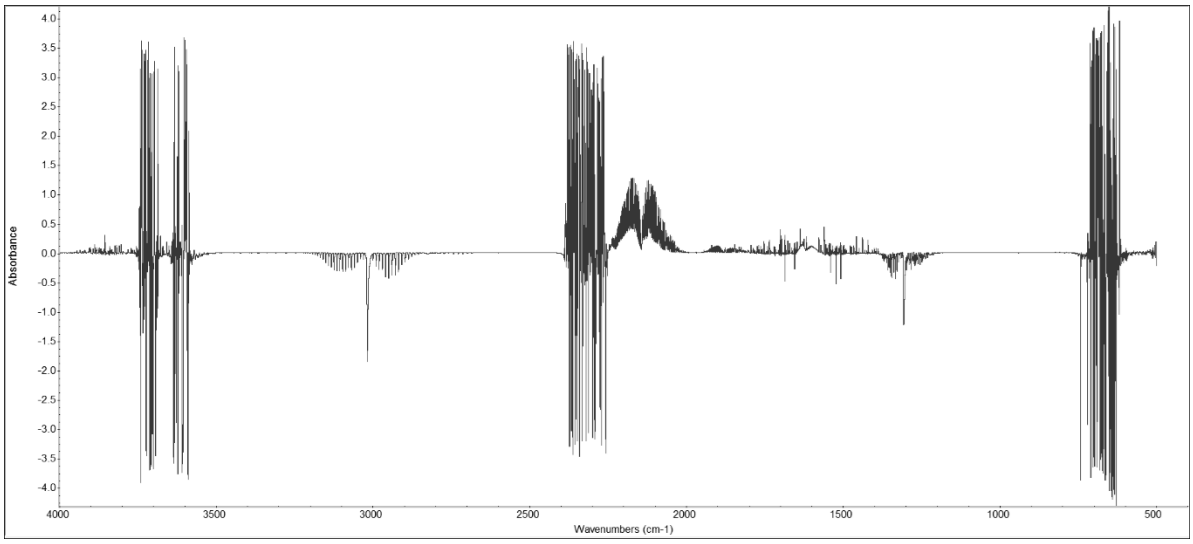

Figure S6. FTIR spectrum of E2, 1:1 mixture CO_2:N_2 with 0.25 % CH_4 added.

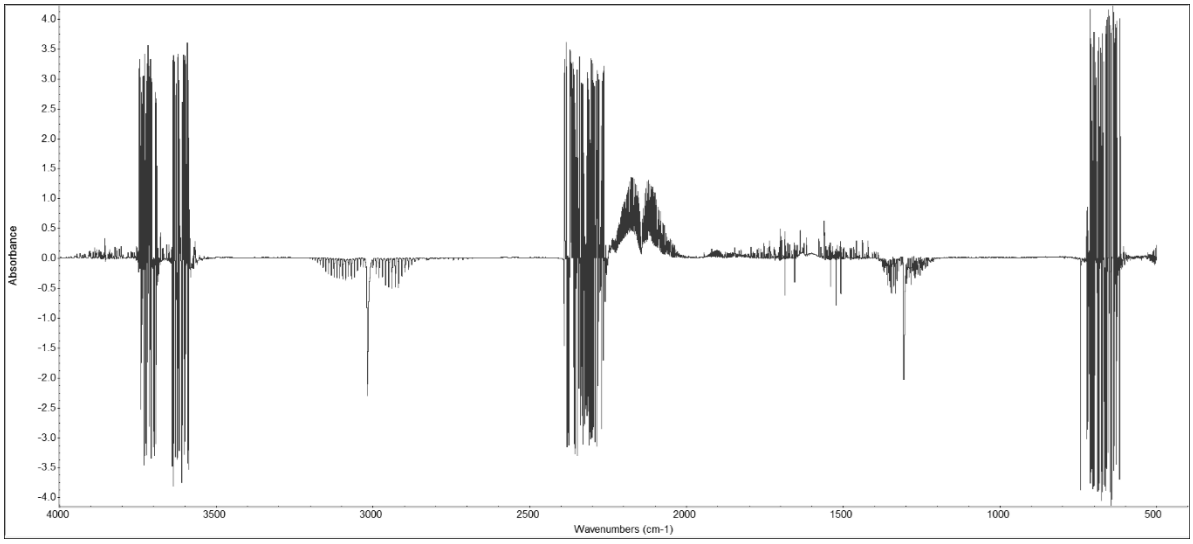

Figure S7. FTIR spectrum of E3, 1:1 mixture CO_2:N_2 with 0.5 % CH_4 added.

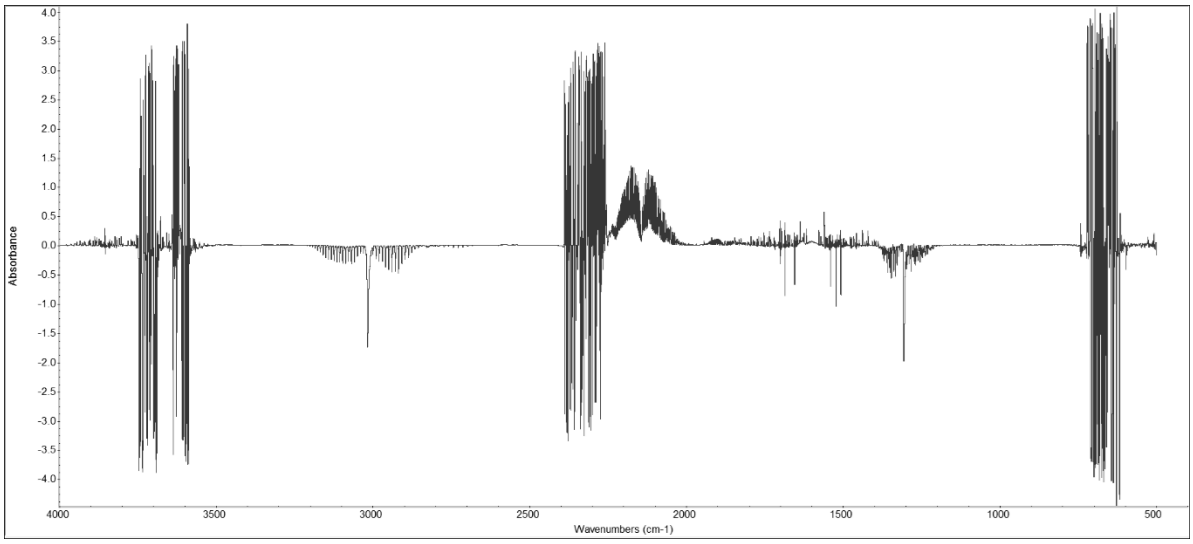

Figure S8. FTIR spectrum of E4, 1:1 mixture CO_2:N_2 with 0.75 % CH_4 added.

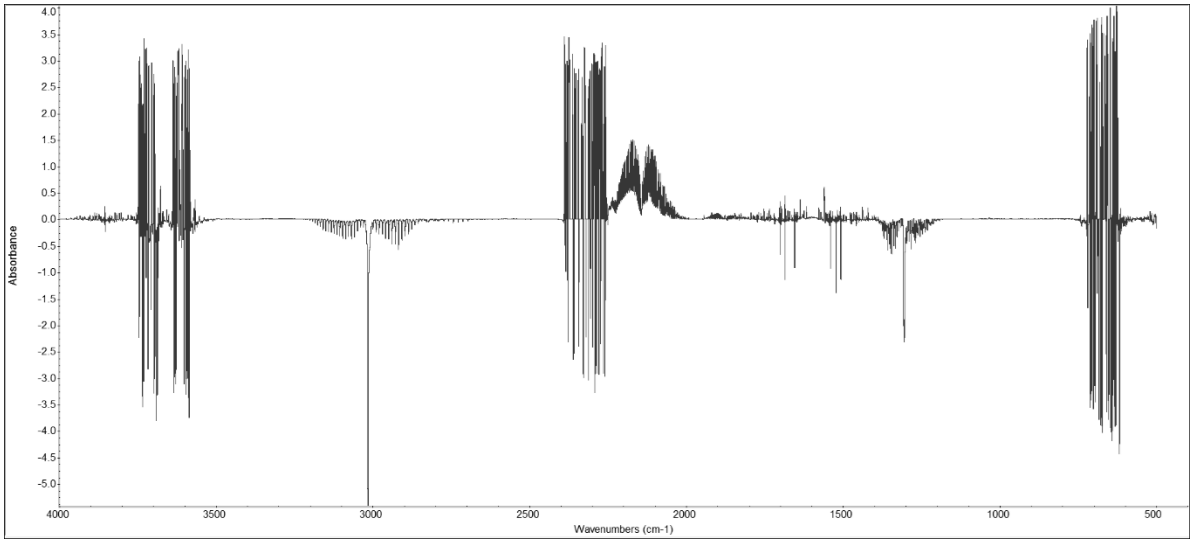

Figure S9. FTIR spectrum of E5, 1:1 mixture CO_2:N_2 with 1.0 % CH_4 added.

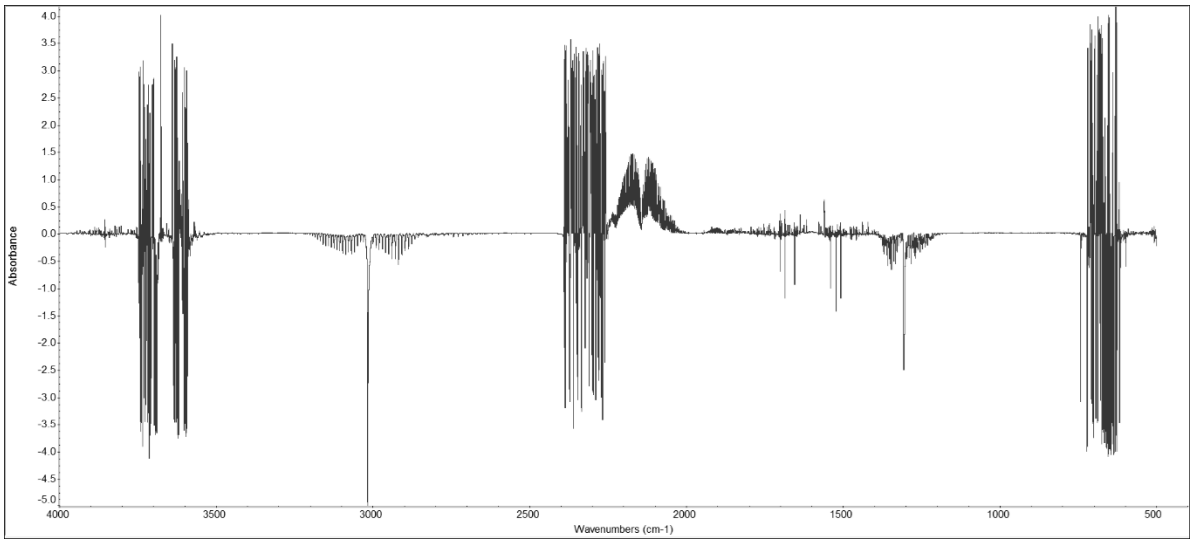

Figure S10. FTIR spectrum of E6, 1:1 mixture CO_2:N_2 with 1.15 % CH_4 added.

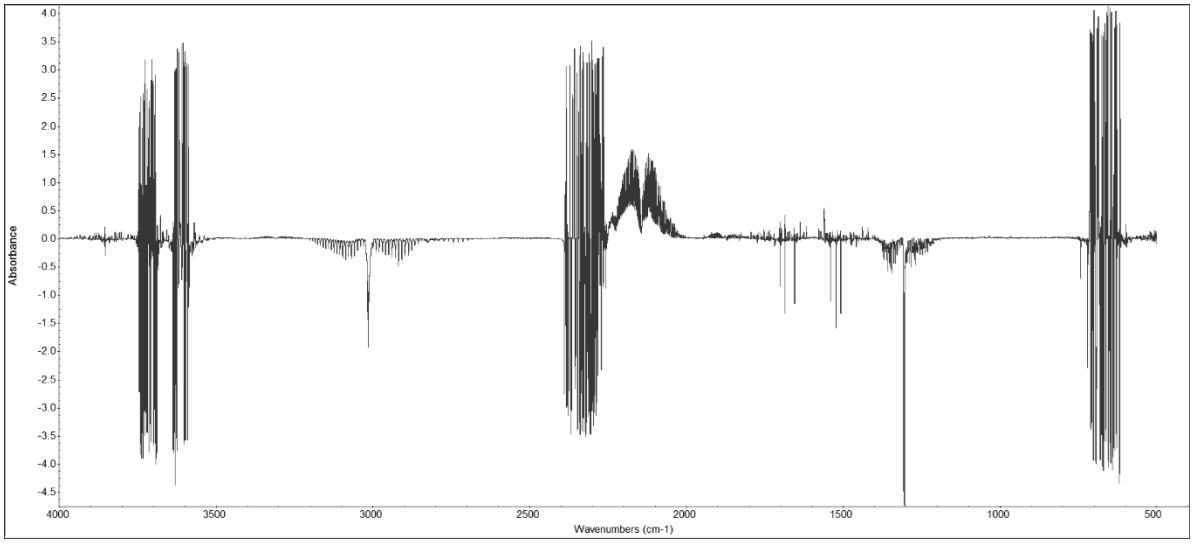

Figure S11. FTIR spectrum of E7, 1:1 mixture CO_2:N_2 with 1.5 % CH_4 added.

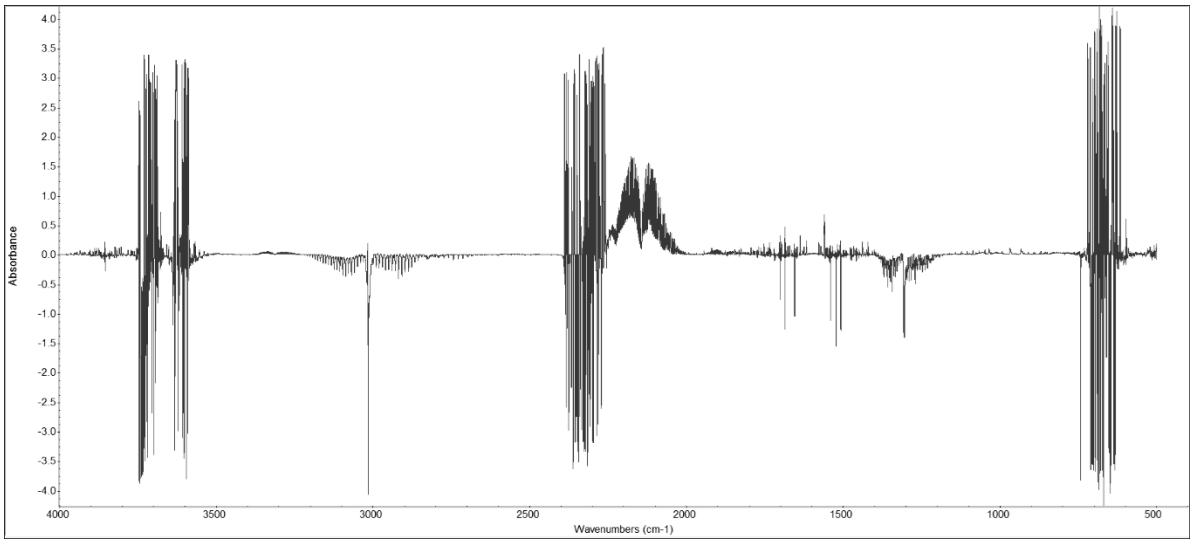

Figure S12. FTIR spectrum of E8, 1:1 mixture CO_2:N_2 with 2.0 % CH_4 added.

2.4. Detailed de-NO_x chemistry

If we first look at the formation of HCN, the key reactions are:

$CH_3 + N \rightarrow HCN + H_2$ $k = 1.40\times10^{-11}$ cm^3 molecule^{-1} s^{-1} at 300 K([1]) (S1)

$CH_2 + N \rightarrow HCN + H$ $k = 5.00\times10^{-11}$ cm^3 molecule^{-1} s^{-1} at 300 K([1]) (S2)

$CN + H \rightarrow HCN$ $k = 1.73\times10^{-10}$ cm^3 molecule^{-1} s^{-1} at 298 K([2]) (S3)

$CH + NO \rightarrow HCN + O$ $k = 2.01\times10^{-10}$ cm^3 molecule^{-1} s^{-1} at 300 K([3]) (S4)

Additionally, from Figure 3b (in the main article), we already know that the HCN concentration increases linearly from the start, indicating that the regular loss processes during the combustion chemistry (leading to prompt NO) appear irrelevant here.[4] This means that instead of being a source of NO (as in the high temperature combustion conditions), in the current low temperature plasma conditions HCN is a sink for the created N species, which also contributes to the suppression of the NO_x formation by trapping the reactive N radicals.

The NH_3 chemistry appears to be quite different. Figure 3b (from the main paper) reveals that the formation of NH_3 occurs after an excess of CH_4 has been added. If we examine the key formation reactions, we notice that they all rely on NH_2:

$NH_2 + NH_2 \rightarrow NH + NH_3$ $k = 5.00\times10^{-11}$ cm^3 molecule^{-1} s^{-1} at 300 K([5]) (S5)

$NH_2 + H_2 \rightarrow H + NH_3$ $k = 2.10\times10^{-12}$ cm^3 molecule^{-1} s^{-1} at 300 K([5]) (S6)

$NH_2 + H \rightarrow NH_3$ $k = 7.36\times10^{-11}$ cm^3 molecule^{-1} s^{-1} at 298 K([6]) (S7)

This shows that, similarly to what occurs in combustion chemistry, NH_x interacts with the NO_x species that are present. When examining the most important reaction rate coefficients for NO and NO_2, we find that the key NO_2 destruction reactions are:

$NO_2 + H \rightarrow NO + OH$ $k = 1.40\times10^{-10}$ cm^3 molecule^{-1} s^{-1} at 298 K([7]) (S8)

$NO_2 + O \rightarrow NO + O_2$ $k = 9.71\times10^{-12}$ cm^3 molecule^{-1} s^{-1} at 298 K([8]) (S9)

$NO_2 + OH \rightarrow HNO_3$ $k = 7.48\times10^{-11}$ cm^3 molecule^{-1} s^{-1} at 298 K([8]) (S10)

$NO_2 + CN \rightarrow NO + NCO$ $k = 8.05\times10^{-11}$ cm^3 molecule^{-1} s^{-1} at 298 K([9]) (S11)

These reactions explain why the NO_2 concentration decreases more rapidly than the NO concentration, as shown in Figure 3a in the main paper, as NO_2 is being converted into NO (and HNO_3).

The following NO formation reactions occur, through HNO as intermediate:

$NH_2 + O \rightarrow H + HNO$ $k = 7.47\times10^{-11}$ cm^3 molecule^{-1} s^{-1} at 300 K([10]) (S12)

$NH_2 + HNO \rightarrow NH_3 + NO$ $k = 3.56\times10^{-12}$ cm^3 molecule^{-1} s^{-1} at 300 K([11]) (S13)

$O + HNO \rightarrow OH + NO$ $k = 5.99\times10^{-11}$ cm^3 molecule^{-1} s^{-1} at 300 K([7]) (S14)

$OH + HNO \rightarrow H_2O + NO$ $k = 1.51\times10^{-11}$ cm^3 molecule^{-1} s^{-1} at 300 K([7]) (S15)

$CH_3 + HNO \rightarrow CH_4 + NO$ $k = 1.04\times10^{-11}$ cm^3 molecule^{-1} s^{-1} at 300 K([12]) (S16)

$CH_3O + HNO \rightarrow CH_3OH + NO$ $k = 5.00\times10^{-11}$ cm^3 molecule^{-1} s^{-1} at 300 K([13]) (S17)

It is important to note that some of the most important NO destruction reactions taking place simultaneously, lead to the formation of HNO, indicating that there is an important equilibrium between NO and HNO:

$NO + H \rightarrow HNO$ $k = 2.43\times10^{-10}$ cm^3 molecule^{-1} s^{-1} at 300 K([7]) (S18)

Additional important NO formation and destruction reactions are:

$N + OH \rightarrow H + NO$ $k = 5.05\times10^{-11}$ cm^3 molecule^{-1} s^{-1} at 300 K([14]) (S19)

$O + NCO \rightarrow CO + NO$ $k = 7.51\times10^{-11}$ cm^3 molecule^{-1} s^{-1} at 500 K([2]) (S20)

$NO + N \rightarrow N_2 + O$ $k = 3.11\times10^{-11}$ cm^3 molecule^{-1} s^{-1} at 300 K([14]) (S21)

$CH + NO \rightarrow HCN + O$ $k = 2.01\times10^{-10}$ cm^3 molecule^{-1} s^{-1} at 300 K([3]) (S22)

As mentioned above, the NH and NH_2 species also play an important role in both the formation and destruction of NO:

$NH + O \rightarrow H + NO$ $k = 1.16\times10^{-10}$ cm^3 molecule^{-1} s^{-1} at 300 K([10]) (S23)

$NO + NH_2 \rightarrow N_2 + H_2O$ $k = 1.24\times10^{-11}$ cm^3 molecule^{-1} s^{-1} at 300 K([15]) (S24)

$NO + NH_2 \rightarrow NNH + OH$ $k = 1.37\times10^{-12}$ cm^3 molecule^{-1} s^{-1} at 300 K([15]) (S25)

$NNH + NO \rightarrow N_2 + HNO$ $k = 5.00\times10^{-13}$ cm^3 molecule^{-1} s^{-1} at 300 K([4]) (S26)

The presence of NH and NCO also create new pathways for the formation of N_2O:

$NO + NCO \rightarrow CO + N_2O$ $k = 1.54\times10^{-11}$ cm^3 molecule^{-1} s^{-1} at 300 K([16]) (S27)

$NO + NH \rightarrow N_2O + H$ $k = 2.87\times10^{-11}$ cm^3 molecule^{-1} s^{-1} at 300 K([17]) (S28)

Whereas the presence of CH actively contributes to the destruction of N_2O through reactions with higher reaction rate coefficients:

$N_2O + CH \rightarrow HCN + NO$ $k = 8.41\times10^{-11}$ cm^3 molecule^{-1} s^{-1} at 300 K([18]) (S29)

$N_2O + CH \rightarrow HCO + N_2$ $k = 8.41\times10^{-11}$ cm^3 molecule^{-1} s^{-1} at 300 K([18]) (S30)

We also find the traditional combustion pathway for the N_2O destruction to be irrelevant:

$N_2O + H \rightarrow N_2 + OH$ $k = 3.18\times10^{-17}$ cm^3 molecule^{-1} s^{-1} at 375 K([19]) (S31)

$N_2O + OH \rightarrow N_2 + HO_2$ $k = 8.09\times10^{-19}$ cm^3 molecule^{-1} s^{-1} at 300 K([7]) (S32)

Finally, the reactions for the formation and destruction of NCO are:

$CH + NO \rightarrow H + NCO$ $k = 3.99\times10^{-11}$ cm^3 molecule^{-1} s^{-1} at 300 K([20]) (S33)

$NO_2 + CN \rightarrow NO + NCO$ $k = 8.05\times10^{-11}$ cm^3 molecule^{-1} s^{-1} at 300 K([9]) (S34)

$O_2 + CN \rightarrow O + NCO$ $k = 2.42\times10^{-11}$ cm^3 molecule^{-1} s^{-1} at 300 K([3]) (S35)

$OH + CN \rightarrow H + NCO$ $k = 7.01\times10^{-11}$ cm^3 molecule^{-1} s^{-1} at 500 K([2]) (S36)

$NO + NCO \rightarrow CO + N_2O$ $k = 1.54\times10^{-11}$ cm^3 molecule^{-1} s^{-1} at 300 K([16]) (S37)

$H + NCO \rightarrow CO + NH$ $k = 8.90\times10^{-11}$ cm^3 molecule^{-1} s^{-1} at 500 K([2]) (S38)

$O + NCO \rightarrow CO + NO$ $k = 7.51\times10^{-11}$ cm^3 molecule^{-1} s^{-1} at 500 K([2]) (S39)

The formed NCO in turn is the precursor to form HNCO through reactions with HCO, HNO and CH_2O, whose production mechanisms have been described earlier:

$HCO + NCO \rightarrow HNCO + CO$ $k = 7.01\times10^{-11}$ cm^3 molecule^{-1} s^{-1} at 500 K([2]) (S40)

$HNO + NCO \rightarrow HNCO + NO$ $k = 3.01\times10^{-11}$ cm^3 molecule^{-1} s^{-1} at 500 K([2]) (S41)

$CH_2O + NCO \rightarrow HNCO + HCO$ $k = 1.00\times10^{-11}$ cm^3 molecule^{-1} s^{-1} at 500 K([2]) (S42)

Again the traditional combustion pathway for (H)NCO formation is irrelevant:

$HCN + O \rightarrow H + NCO$ $k = 5.03\times10^{-18}$ cm^3 molecule^{-1} s^{-1} at 300 K([21]) (S43)

$NCO + H_2 \rightarrow HNCO + H$ $k = 7.68\times10^{-18}$ cm^3 molecule^{-1} s^{-1} at 300 K([22]) (S44)

3. References

1 D. Toublanc, J. P. Parisot, J. Brillet, D. Gautier, F. Raulin and C. P. McKay, *Icarus*, 1995, **113**, 2–26.

2 W. Tsang, *J. Phys. Chem. Ref. Data*, 1992, **21**, 753–791.

3 D. L. Baulch, C. J. Cobos, R. A. Cox, P. Frank, G. Hayman, T. Just, J. A. Kerr, T. Murrells, M. J. Pilling, J. Troe, R. W. Walker and J. Warnatz, *J. Phys. Chem. Ref. Data*, 1994, **23**, 847–1033.

4 J. A. Miller and C. T. Bowmans, *Prog. Energy Combust. Sci.*, 1989, **15**, 287–338.

5 R. Dorai, University of Illinois, 2002.

6 K. Schofield, *J. Phys. Chem. Ref. Data*, 1973, **2**, 25–84.

7 W. Tsang and J. T. Herron, *J. Phys. Chem. Ref. Data*, 1991, **20**, 609–663.

8 R. Atkinson, D. L. Baulch, R. A. Cox, R. F. Hampson, J. A. Kerr, M. J. Rossi and J. Troe, *J. Phys. Chem. Ref. Data*, 1997, **26**, 1329–1499.

9 J. Park and J. F. Hershberger, *J. Chem. Phys.*, 1993, **99**, 3488–3493.

10 N. Cohen and K. R. Westberg, *J. Phys. Chem. Ref. Data*, 1991, **20**, 1211–1311.

11 A. J. Zhang, A. M. Zhu, J. Guo, Y. Xu and C. Shi, *Chem. Eng. J.*, 2010, **156**, 601–606.

12 Y. M. Choi and M. C. Lin, *Int. J. Chem. Kinet.*, 2005, **37**, 261–274.

13 G. E. McGraw and H. S. Johnston, *Int. J. Chem. Kinet.*, 1969, **I**, 89–104.

14 R. Atkinson, D. L. Baulch, R. A. Cox, R. F. Hampson, J. A. Kerr (Chairman) and J. Troe, *J. Phys. Chem. Ref. Data*, 1989, **18**, 881–1097.

15 J. Park and M. C. Lin, *J. Phys. Chem. A*, 1999, **103**, 8906–8907.

16 M. C. Lin, Y. He and C. F. Melius, *J. Phys. Chem.*, 1993, **97**, 9124–9128.

17 J. W. Bozzelli, A. Y. Chang and A. M. Dean, *Symp. Combust.*, 1994, **25**, 965–974.

18 S. Zabarnick, J. W. Fleming and M. C. Lin, *Int. J. Chem. Kinet.*, 1989, **21**, 765–774.

19 N. L. Arthur, I. A. Cooper and Y. M. Gershenzon, *J. Chem. Soc. - Faraday Trans.*, 1997, **93**, 3485–3490.

20 A. Bergeat, T. Calvo, N. Daugey, J. C. Loison and G. Dorthe, *J. Phys. Chem. A*, 1998, **102**, 8124–8130.

21 R. A. Perry and C. F. Melius, *Symp. Combust.*, 1985, **20**, 639–646.

22 M. T. Nguyen, D. Sengupta, L. Vereecken, J. Peeters and L. G. Vanquickenborne, *J. Phys. Chem.*, 1996, **100**, 1615–1621.